Fission-Fragment Energy-Correlation Measurements for the Thermal-Neutron Fission of ^{239}Pu and ^{241}Pu†

J. N. Neiler,* F. J. Walter,* and H. W. Schmitt

Oak Ridge National Laboratory, Oak Ridge, Tennessee

(Received 4 April 1966)

Fission-fragment mass and energy distributions and mass-versus-energy correlations have been obtained for ^{239}Pu and ^{241}Pu thermal-neutron-induced fission. Silicon surface-barrier detectors were used in energy-correlation measurements; absolute fragment energies were obtained by means of a recently developed mass-dependent energy calibration. Average total fragment kinetic energies before neutron emission are found to be 177.7±1.8 MeV for ^{239}Pu and 179.6±1.8 MeV for ^{241}Pu. Detailed experimental results are given and compared with those of other experiments. Observed fine structure in the fragment mass distribution and in the average total fragment kinetic energy as a function of mass is correlated with the energetically preferred even-even nucleon configurations in the fragments. New determinations of the root-mean-square width of the total-kinetic-energy distribution as a function of fragment mass show structure which also appears to be correlated with the energetically preferred even-even fragment configurations. Fission neutron and gamma-ray data of other experiments are used with the new fragment kinetic energies presented here to examine the total energy balance for fission for the two cases studied. A comparison of the two mass distributions shows the heavy-fragment groups almost superimposed; the light-fragment groups are separated almost uniformly by 2 amu.

I. INTRODUCTION

FISSION-fragment energy-correlation experiments (more properly called pulse-height correlation experiments) have been carried out for the thermal-neutron induced fission of ^{239}Pu and ^{241}Pu. Mass and energy distributions and mass-energy correlations have been obtained. Silicon surface-barrier detectors were used to detect the fragments; correlated pulse amplitudes were recorded in two parameters of 128 channels each.

These experiments are part of a series of such experiments which have been carried out to study the mass and energy distributions and mass-energy correlations for low-excitation fission; particular attention has been given to the determination of absolute fragment energies. A previous publication[1] gives results for ^{252}Cf spontaneous fission and ^{235}U thermal-neutron-induced fission.

In Ref. 1 we have given a description of the experiments and a development of the analysis of such experiments in some detail. Since these apply in most respects to the particular measurements reported here, the experimental method will be outlined only briefly; we refer entirely to Ref. 1 for details of the analysis. Table I, essentially reproduced from Ref. 1, gives a list of definitions and symbols used in these discussions.

Previous energy measurements of fragments from thermal-neutron-induced fission of plutonium include (1) ionization chamber measurements, for example earlier double-chamber measurements by Brunton and Thompson[2] and more recent measurements by Apalin

et al.,[3] and (2) time-of-flight measurements, including early single- and double-velocity measurements by Leachman[4] and Stein,[5] respectively, and recent double-velocity measurements by Milton and Fraser.[6] Previous studies of plutonium thermal-neutron fission involving solid-state detectors have been reported by Gibson *et al.*[7] and by Walter *et al.*[8] Mass distributions have been obtained from some of the kinetic measurements; these have been essentially pre-neutron-emission mass distributions. Post-neutron-emission mass distributions have in general been obtained from radiochemical and mass spectrometric measurements; mass yields have been compiled for ^{239}Pu by Fickel and Tomlinson,[9] Katcoff,[10] and Walker[11] and for ^{241}Pu by Farrar *et al.*[12]

In a comparison of results of the present experiment with those of the most recent double-velocity experiments, small but significant discrepancies of several percent (up to $\sim 10\%$ at symmetry) have been observed in fragment kinetic energies. These discrepancies are now understood, and have led to improved fragment kinetic energy values, as discussed below.

[1] H. W. Schmitt, J. H. Neiler, and F. J. Walter, Phys. Rev. 141, 1146 (1966).

[2] D. C. Brunton and W. B. Thompson, Can. J. Res. 28A, 498 (1950).

[3] V. F. Apalin, Yu. N. Gritsyuk, I. E. Kutikov, V. I. Lebedev, and L. A. Mikaelyan, Nucl. Phys. 71, 553 (1965).

[4] R. B. Leachman, Phys. Rev. 87, 444 (1952).

[5] W. E. Stein, Phys. Rev. 108, 94 (1957).

[6] J. C. D. Milton and J. S. Fraser, Can. J. Phys. 40, 1626 (1962); Phys. Rev. Letters 7, 67 (1961).

[7] W. M. Gibson, T. D. Thomas, and G. L. Miller, Phys. Rev. Letters 7, 65 (1961).

[8] F. J. Walter, H. W. Schmitt, and J. H. Neiler, Phys. Rev. 133, B1500 (1964).

[9] H. R. Fickel and R. H. Tomlinson, Can. J. Phys. 37, 916 (1959); 37, 926 (1959).

[10] S. Katcoff, Nucleonics 18, 201 (1960).

[11] W. H. Walker, Chalk River Report No. CRRP-913, 1960 (unpublished).

[12] H. Farrar, W. B. Clarke, H. G. Thode, and R. H. Tomlinson, Can. J. Phys. 42, 2063 (1964).

*	Denotes quantities for pre-neutron-emission fragments.
$\langle \ \rangle$ or bar	Denotes average quantities, as indicated.
A	Mass of fissioning nucleus.
a_i, a_i', b_i, b_i'	Constants in energy calibration equation for silicon solid-state detectors.
B_{ni}	Binding energy of nth neutron emitted from ith fragment.
$E_{ki}*$	Pre-neutron-emission kinetic energy of ith fragment.
E_{ki}	Post-neutron-emission kinetic energy of ith fragment.
E_K*	Total pre-neutron-emission fragment kinetic energy.
E_K	Total post-neutron-emission fragment kinetic energy.
E_{Ri}	Center-of-mass recoil energy of neutron-emitting fragment.
$E_{xi}*$	Pre-neutron-emission excitation energy of ith fragment.
$E_{xT}*$	Total pre-neutron-emission fragment excitation energy (both fragments).
$E_{\gamma i}$	Gamma decay energy for ith fragment.
$E_{\gamma T}$	Total fragment gamma decay energy (both fragments).
FWHM	Full width at half maximum.
H	Subscript indicating heavy fragment.
i	$i=1, 2$; subscript index indicating first or second fragment, corresponding to first or second detector.
L	Subscript indicating light fragment.
m_i*	Pre-neutron-emission mass of ith fragment.
m_i	Post-neutron-emission mass of ith fragment.
N	Number of events or counts.
Q	Total energy available for nuclear reaction (fission).
x_i	Channel number for ith fragment, corresponding to pulse height from ith detector.
Z, N	Proton, neutron number of nucleus.
η_i	Average center-of-mass kinetic energy of neutrons emitted from ith fragment.
μ_1, μ_2	Provisional mass, defined by $\mu_1 = A E_{k2}/E_K$, $\mu_2 = A E_{k1}/E_K$.
ν_i	Number of electrons emitted from ith fragment.
ν_T	Total number of neutrons emitted (both fragments).
σ	Root-mean-square width, square root of second central moment; variable is indicated in subscript.

II. METHOD AND APPARATUS

The target consisted of a thin fissile deposit on a thin backing foil in which the fragment energy loss was less than ~ 5 MeV. In the case of ^{239}Pu, the deposit consisted of ~ 20 μg per cm^2 PuO$_2$, vacuum evaporated onto a nickel backing ~ 70 μg per cm^2 thick. The ^{241}Pu was prepared in the form PuF$_4$; a deposit ~ 20 μg per cm^2 thick was vacuum evaporated onto a carbon film about 20 μg per cm^2 thick. In each case, the thin foils spanned an aperture 2 cm in diameter; the neutron beam was collimated to a diameter slightly less than 1 cm, so that it was not incident on the mounting frame or any other part inside the vacuum chamber. Contributions from thermally fissionable impurities in the samples (estimated from mass spectrometric analyses) were less than 0.8% in both cases; no corrections for impurity contributions have been made.

Two surface-barrier detectors were mounted face to face on opposite sides of the target, as indicated in Fig. 1 of Ref. 1. The detectors were fabricated from n-type silicon of nominal resistivity 500 Ω cm and were 4 cm^2 in area. The fragment collimators were $\frac{1}{16}$-in.-thick aluminum, and the apertures were rounded to minimize scattering and low-energy tailing. The detectors were

operated in the "saturation region" of the pulse-height-versus-bias curve, and their performances were similar to those reported for the detectors of Ref. 1.

Details of the electronic system used in these experiments are given in an earlier publication[13]; particular attention was given to the elimination of pile-up pulses, including fission-on-fission and alpha-on-fission events. Data were accumulated event-by-event on punched paper tape in 128×128 channels. Each of the experiments reported here contains $\sim 10^6$ events, although a number of similar runs were made to check various experimental effects and to establish optimum conditions for the experiments.

III. RESULTS FOR ^{239}Pu THERMAL-NEUTRON FISSION

The pulse-height correlation data array $N(x_1, x_2)$ is shown in Fig. 1. Data were obtained in 128×128 channels, and a total of $\sim 10^6$ events are included. The numbers labeling the contours indicate the number of events per cell (1 channel×1 channel). Lines of constant total kinetic energy E_K and of constant provisional mass μ_1 or μ_2 are included. (μ_1 and μ_2 are the provisional fragment masses calculated from measured energies and assumed momentum conservation—see Table I.) A transformation to the array $N(\mu_1, E_K)$ was carried out; this array is shown in Fig. 2. Numbers labeling the contours in this figure indicate the number of events per MeV per amu. In both Fig. 1 and Fig. 2, the numbers of events per cell have been entered outside the 10 contours in order to show the locations of rarer events.

The absolute energy calibration was obtained from an independent comparison measurement of fragment pulse-height spectra for ^{252}Cf and ^{239}Pu; the method of calibration has been described previously[14] and contains a mass dependence in pulse height response. The calibration constants of Ref. 14 were used to derive a similar set of constants for ^{239}Pu, which in turn were used to calibrate the present experiment.

Complete two-dimensional data giving ν as a function of fragment mass and kinetic energy would be required to construct lines of constant m_1* or E_K* in the above arrays or to construct the array $N(m_1*, E_K*)$. Such

[13] C. W. Williams, H. W. Schmitt, F. J. Walter, and J. H. Neiler, Nucl. Instr. Methods **29**, 205 (1964).

[14] H. W. Schmitt, W. E. Kiker, and C. W. Williams, Phys. Rev. **137**, B837 (1965). (The method of detector calibration is contained in Appendix II.) Further discussion of the energy calibration and response of solid-state detectors, based on fission-fragment and heavy-ion measurements, have been reported: see H. W. Schmitt, W. M. Gibson, J. H. Neiler, F. J. Walter, and T. D. Thomas, *Symposium on the Physics and Chemistry of Fission, 1965* (International Atomic Energy Agency, Vienna, 1965), Vol. I, p. 531. A method of evaluation of detector quality has also been reported by H. W. Schmitt and F. Pleasonton, Nucl. Instr. Methods, **40**, 204 (1966).
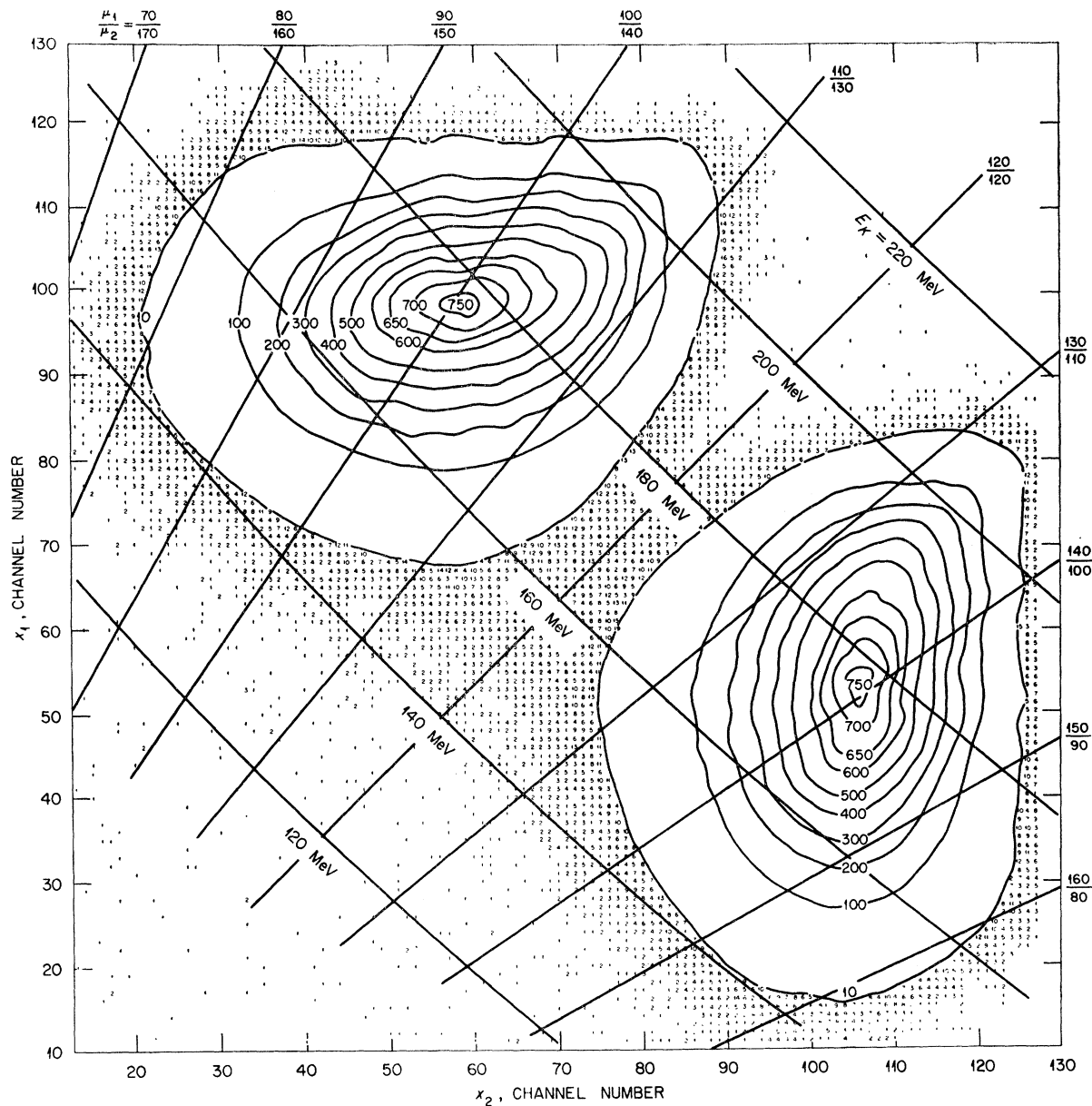
FIG. 1. Pulse-height correlation data array $N(x_1,x_2)$ for ^{239}Pu thermal-neutron-induced fission. This array contains 0.97×16^6 events. The numbers labeling the contours and those outside the 10 contours indicate the number of events per cell (1 channel$\times$1 channel). Lines of constant μ_1/μ_2 and E_K are shown.

data are being obtained[15]; however, for general application to these and other energy correlation experiments we have taken the approach described in Ref. 1, that is, we derive the parameters and functions of interest from the $N(\mu_1,E_K)$ array and account for the effects of neutron emission in a separate step. The relation between μ_1 and m_1^*, based on the average neutron emission data of Apalin et al.,[3] is given in Fig. 3(c).

---

[15] J. C. D. Milton and J. S. Fraser (private communication); data for ^{235}U and ^{233}U have been published in Symposium on the Physics and Chemistry of Fission (International Atomic Energy Agency, Vienna, 1965), Vol. II, p. 39.

The fragment-mass distribution obtained from the present experiment is shown in Fig. 3(a). For comparison, both the provisional-mass distribution $N(\mu)$ and the pre-neutron-emission mass distribution $N(m^*)$ are shown; the latter is obtained from $N(\mu)$ and $\nu(m^*)$, as indicated in Ref. 1. No resolution corrections are included in these curves. Similarly, the average total kinetic energy $\langle E_K(\mu)\rangle$, based on the provisional masses, is shown in Fig. 3(b) together with the total pre-neutron-emission kinetic energy $\langle E_K^*(m^*)\rangle$. The quantities $N(\mu)$ and $\langle E_K(\mu)\rangle$ are obtained from the $N(\mu_1,E_K)$ array and are independent of neutron emission data.
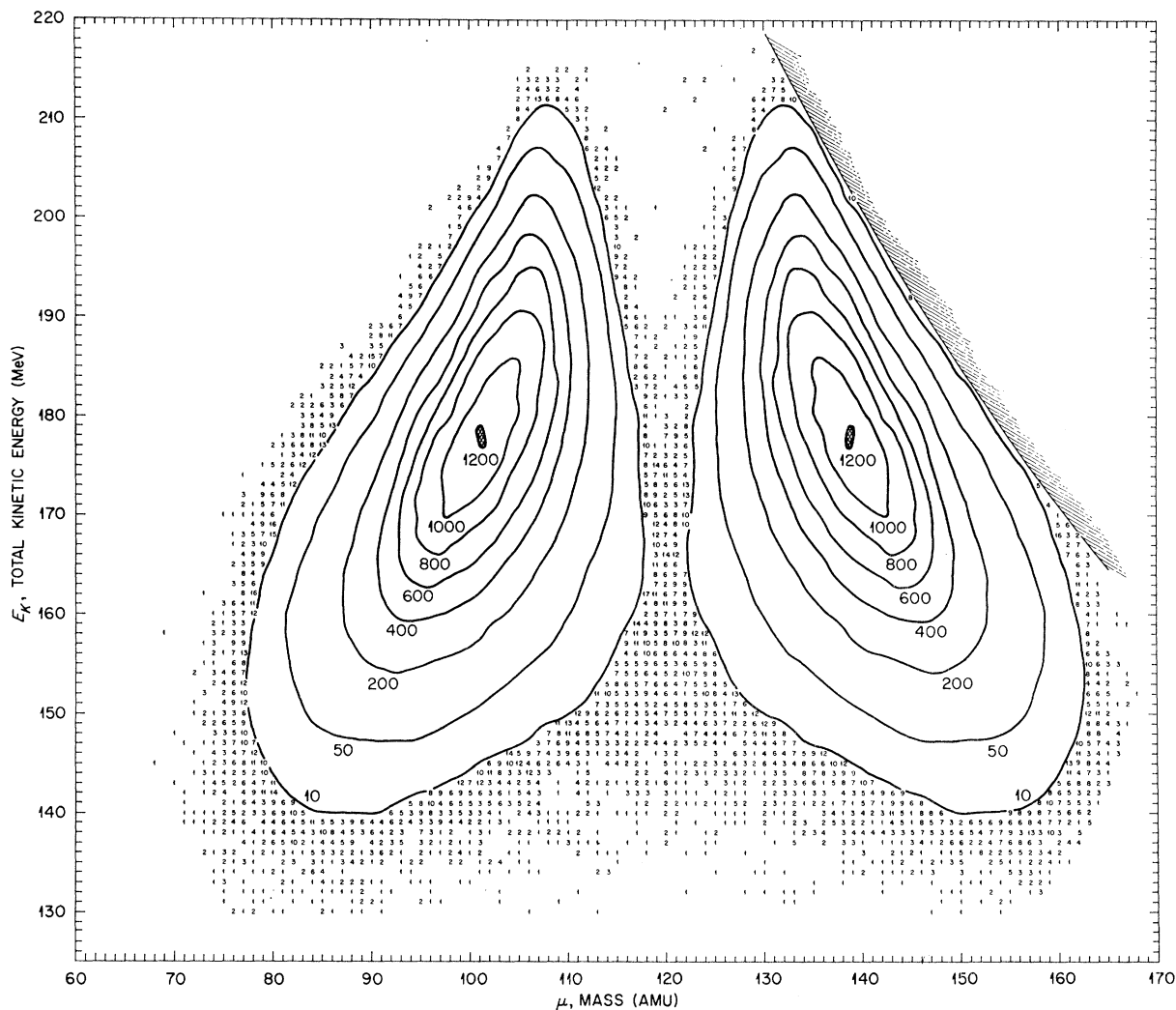
FIG. 2. Provisional mass-versus-total kinetic energy array $N(\mu, E_K)$ for ^{239}Pu thermal-neutron fission. Numbers labeling the contours and those entered outside the 10 contours indicate the number of events per cell (1 amu×1 MeV). The curve in the upper-right-hand portion of the array corresponds to the vertical line x_2=channel 127 in Fig. 1, and represents the upper limit of data acquisition in x_2.

In Fig. 4(a) we show the dispersion-corrected pre-neutron-emission mass distribution for ^{239}Pu from the present experiment, compared with the post-neutron-emission mass distribution determined from radiochemical and mass spectrometric measurements.[9-11] The dispersion correction includes the effects of neutron emission and of detector resolution as discussed in Ref. 1, where an equation for the over-all mass resolution is also given. In applying this correction, the method of second derivatives involving five-point least-squares fits to second-degree polynomials (as described in Ref. 14) was used. The differences in the two curves of Fig. 4(a) are understood in terms of the variation of $\nu(m^*)$ in each fragment group, as discussed previously, principally by Terrell[16] for this and other cases of low-

excitation fission. It is also observed in Fig. 4(a) that the yield in the valley of the present mass distribution is comparable with that of radiochemical data. The observed fine structure is discussed in Sec. V and a detailed comparison of the ^{239}Pu and ^{241}Pu mass distributions is discussed in Secs. V and VI.

The average single-fragment pre-neutron-emission energy is shown as a function of fragment mass in Fig. 4(b); also the average total pre-neutron-emission kinetic energy is plotted as a function of fragment mass. The total-kinetic-energy curve of Milton and Fraser[6] is shown for comparison. The discrepancy is 2 to 4 MeV over most of the mass range, increasing to ~17 MeV at symmetry, and is now understood in terms of the effect of fragment scattering from the walls of the flight tubes in the double-velocity experiment. The possible effects of scattering were discussed by Milton and Fraser

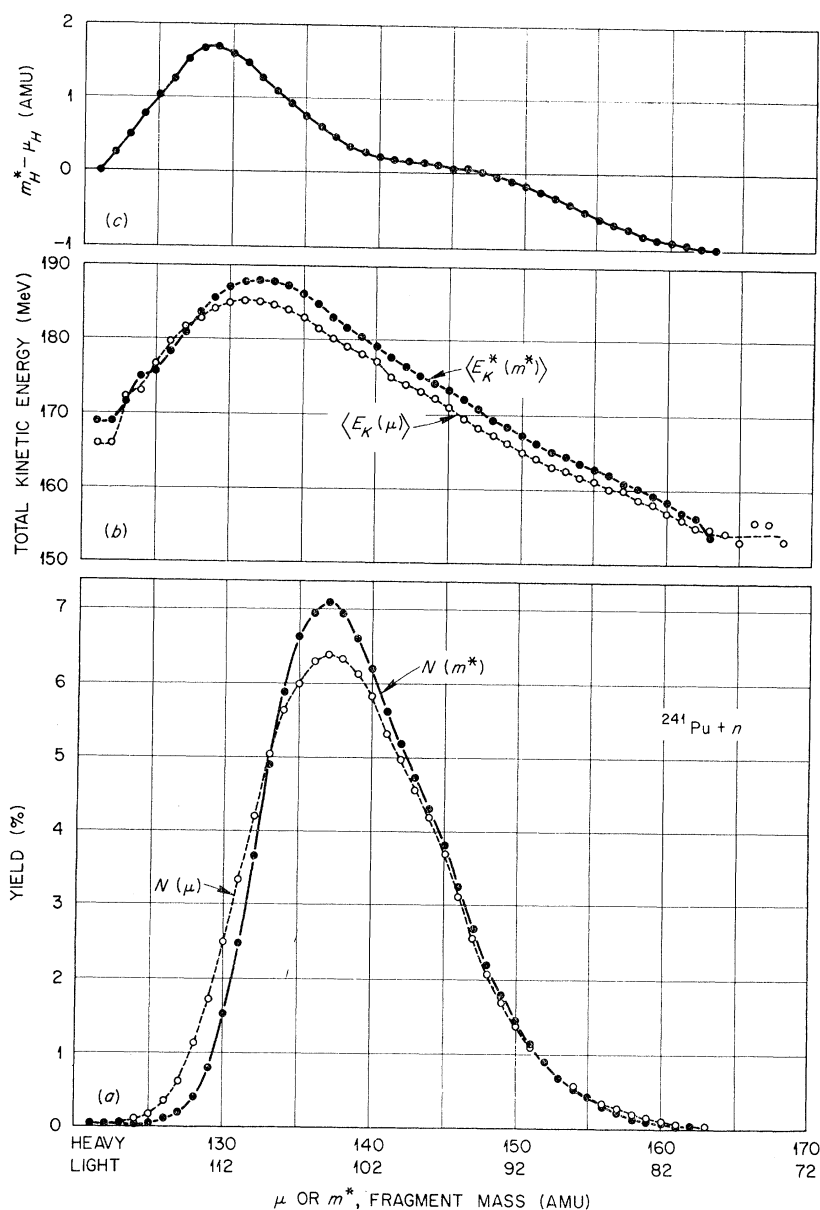[16] J. Terrell, Phys. Rev. **127**, 880 (1962).

FIG. 3. Interim results for ^{239}Pu thermal-neutron fission. (a) Provisional mass distribution $N(\mu)$ and pre-neutron-emission mass distribution $N(m^*)$. Statistical uncertainties are small; the peaks contain $>30\,000$ counts per amu. No corrections for resolution have been included. (b) $\langle E_K(\mu)\rangle$ and $\langle E_K{}^*(m^*)\rangle$. (c) $m_H{}^* - \mu_H$ versus $m_H{}^*$.

in Ref. 6, but the surprisingly large magnitude of the probability for fragment scattering at small angles to a surface was only recently found explicitly in the measurements of Engelkemeier.[17] Such scattering produces tailing toward lower velocities and energies, and thus somewhat broadens the derived mass distributions and alters the average total kinetic energies, i.e., decreases them over most of the mass range.[18] The general shape of the kinetic energy curve of Milton and Fraser,

however, is not qualitatively different from that of the present curve; therefore many of the conclusions and points of discussion made by these authors on the basis of the qualitative trends remain applicable.

The rms width σ_{E_K} of the total-kinetic-energy distribution as a function of fragment mass is plotted in Fig. 4(c). The variation in ν as a function of total kinetic energy for a given mass division was neglected in computing this quantity. That is, the quantity $\sigma_{E_K}{}^2$, where

$$\sigma_{E_K}{}^2 = \langle E_K{}^2\rangle - \langle E_K\rangle^2, \tag{1}$$

was calculated as a function of μ, from the $N(\mu_1, E_K)$ array. The value of μ_1 corresponding to an integral

[17] D. Engelkemeier and G. N. Walton, Phys. Rev. **146**, 304 (1966); also private communication.

[18] This effect was also discussed in Ref. 1 in connection with the ^{252}Cf and ^{235}U results. Discussions with J. S. Fraser and J. C. D. Milton on this point are again gratefully acknowledged.
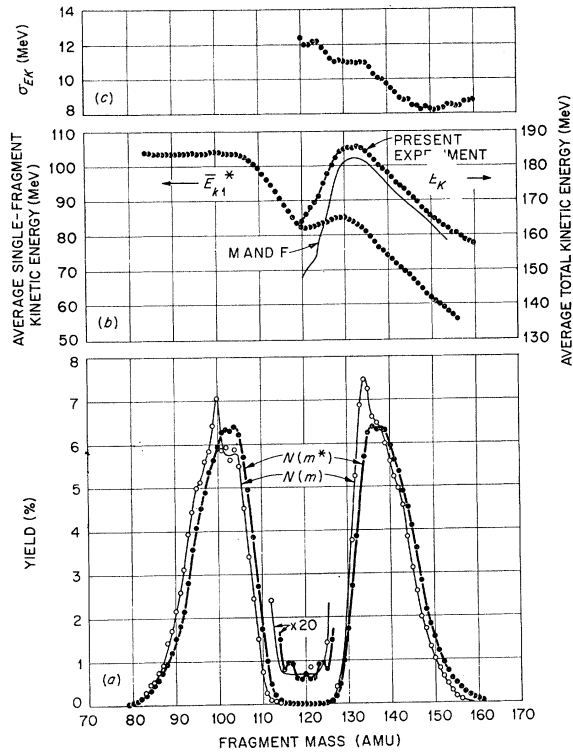
FIG. 4. Results for ²³⁹Pu thermal-neutron fission. (a) Pre-neutron-emission mass distribution corrected for resolution (closed circles); the post-neutron-emission mass distribution points (open circles) are from Fickel and Tomlinson (Ref. 9) and in the symmetric region from Katcoff (Ref. 10). The smooth curve at symmetry is from Walker (Ref. 11). (b) Average single-fragment and total pre-neutron-emission kinetic energy as a function of fragment mass. The curve of Milton and Fraser (Ref. 6) is shown for comparison; see text for discussion. (c) Root-mean-square width of total-kinetic-energy distribution as a function of fragment mass.

value of m_1^* was found, and $\sigma_{E_K}^2$ at this value was obtained by interpolation. The square root of this value of $\sigma_{E_K}^2$ is plotted as a function of m_1^* in Fig. 4(c).

A list of average total kinetic energies, light- and heavy-fragment energies and masses, and of the distribution widths is given in Table II. The "dip" in average total kinetic energy at symmetry, defined as the difference between the maximum value of $\bar{E}_K^*(m^*)$

TABLE II. Mean values and rms widths of the distributions.

Quantity	²³⁹Pu +$n_{thermal}$ This work	²³⁹Pu +$n_{thermal}$ Milton & Fraser[a]	²⁴¹Pu +$n_{thermal}$ This work
$\langle E_K^* \rangle$ (MeV)	177.7 ±1.8	174.4±1.7	179.6±1.8
$\sigma_{E_K}^*$ (MeV)	(11.09)[b]	12.2	(11.46)[b]
$\langle E_L^* \rangle$ (MeV)	103.2 ±1.0	101.8±1.0	103.2±1.0
$\langle E_H^* \rangle$ (MeV)	74.5 ±0.8	73.2 +0.7	76.3±0.8
$\langle m_L^* \rangle$ (amu)	100.34	100.23	102.58
$\langle m_H^* \rangle$ (amu)	139.66	139.77	139.42
$\sigma_{m_L}^*$ or $\sigma_{m_H}^*$ (amu)	6.01	6.36	5.71

[a] Milton and Fraser, Ref. 6 and Errata.
[b] This is σ_{E_K} calculated from $N(\mu,E_K)$ and may not be exactly equal to $\sigma_{E_K}^*$.

and the value at symmetry, is found from the present experiment to be 22 MeV.

IV. RESULTS FOR ²⁴¹Pu THERMAL-NEUTRON FISSION

The pulse-height correlation data array $N(x_1,x_2)$ is shown in Fig. 5. Data were obtained in 128×128 channels and a total of ∼10⁶ events are included in this array. The numbers labeling the contours indicate the number of events per cell (1 channel×1 channel), and lines of constant total kinetic energy E_K and of constant provisional mass μ_1 or μ_2 are included. A transformation to the array $N(\mu_1,E_K)$ was carried out; this array is shown in Fig. 6. Numbers labeling the contours in this figure indicate the number of events per MeV-amu. In both Fig. 5 and Fig. 6, the actual numbers of events per cell have been entered outside the 10 contours in order to show the locations of rarer events. The absolute-energy calibrations were obtained by the method indicated above for ²³⁹Pu (Sec. III).

As in the case of ²³⁹Pu, we derive the parameters and functions of interest from the $N(\mu_1,E_K)$ array, then account for the effects of neutron emission in a separate step. To our knowledge, however, there are no experimental neutron-emission data for ²⁴¹Pu thermal-neutron fission. Therefore, we have examined the function we require, i.e., $\nu(m^*)$, as experimentally determined for other target nuclei and attempted to derive by interpolation a reasonable function $\nu(m^*)$ for ²⁴¹Pu. The data involved in this procedure and the resulting $\nu(m^*)$ assumed in the present analysis for ²⁴¹Pu are shown in Fig. 7. The ²³⁵U and ²³⁹Pu data are those of Apalin et al.[3] and the ²⁵²Cf data are those of Bowman et al.[19] The deviations in our assumed $\nu(m^*)$ for ²⁴¹Pu relative to the ²³⁹Pu experimental data, are small over most of the mass range. The relationship between μ_1 and m_1^* based on this assumed $\nu(m^*)$ is shown in Fig. 8(c).

In Fig. 8(a) the provisional-mass distribution $N(\mu)$ and the deduced pre-neutron-emission mass distribution $N(m^*)$ are shown; no resolution corrections are included in these curves. Similarly, the quantities $\langle E_K(\mu) \rangle$ and $\langle E_K^*(m^*) \rangle$ are shown in Fig. 8(b).

The mass-energy results for ²⁴¹Pu are summarized in Fig. 9. The dispersion-corrected (see Sec. III) pre-neutron-emission mass distribution from the present experiment is shown in Fig. 9(a). The post-neutron-emission heavy-fragment distribution is that of Farrar et al.[12] The differences observed here are consistent with the expected variation in $\nu(m^*)$ in the heavy-fragment group, although in the mass regions 130–133 amu and above ∼146 amu the two distributions seem to be closer together than in the case of ²³⁹Pu. Fine structure is observed again in this distribution; we shall discuss it in more detail in Sec. V. A detailed comparison of the

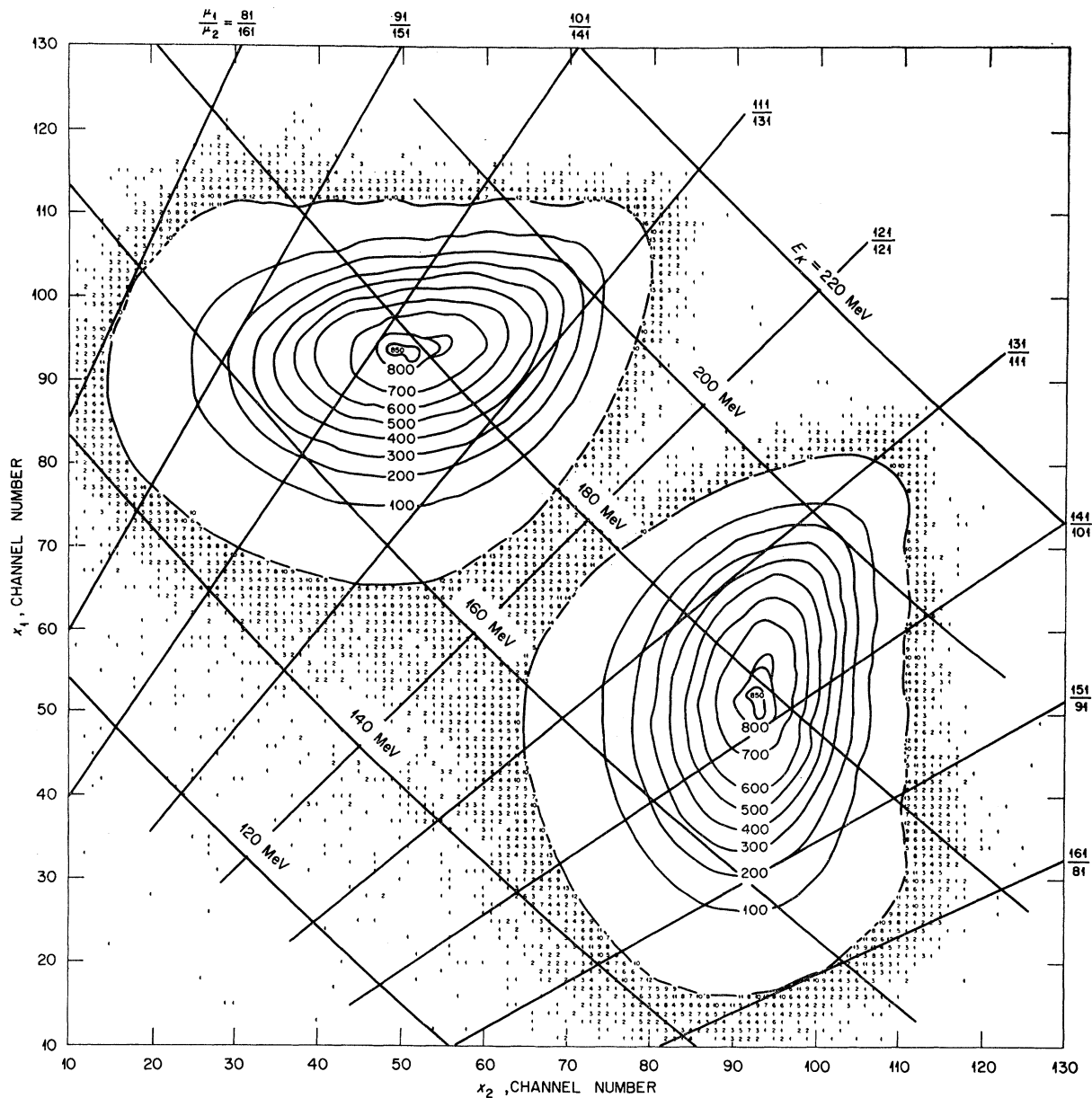[19] H. R. Bowman, J. C. D. Milton, S. G. Thompson, and W. J. Swiatecki, Phys. Rev. **129**, 2133 (1963).

FIG. 5. Pulse-height correlation data array $N(x_1,x_2)$ for ^{241}Pu thermal-neutron-induced fission. This array contains 0.97×10^6 events. The numbers labeling the contours and those outside the 10-contours indicate the number of events per cell (1 channel$\times$1 channel). Lines of constant μ_1/μ_2 and E_K are shown.

^{239}Pu and ^{241}Pu distributions is contained in Secs. V and VI.

The average-total and single-fragment pre-neutron-emission kinetic energies as functions of fragment mass $\langle E_K^*(m^*)\rangle$ and $\langle E_{k1}^*(m^*)\rangle$, are shown in Fig. 9(b). The rms width σ_{E_K} of the total-kinetic-energy distribution as a function of fragment mass is plotted in Fig. 9(c). The method of calculation of this quantity is as indicated in Sec. III.

A list including average total kinetic energy, average light- and heavy-fragment kinetic energies and masses,

and widths of the distributions is given in Table II. The "dip" in average total kinetic energy at symmetry is found to be 20 MeV.

V. ENERGY BALANCE AND FINE STRUCTURE

The total energy available for fission into a given mass pair m_1^*, m_2^* (i.e., the Q value, defined as is usual for nuclear reations) appears as kinetic and excitation energy of the fragments:

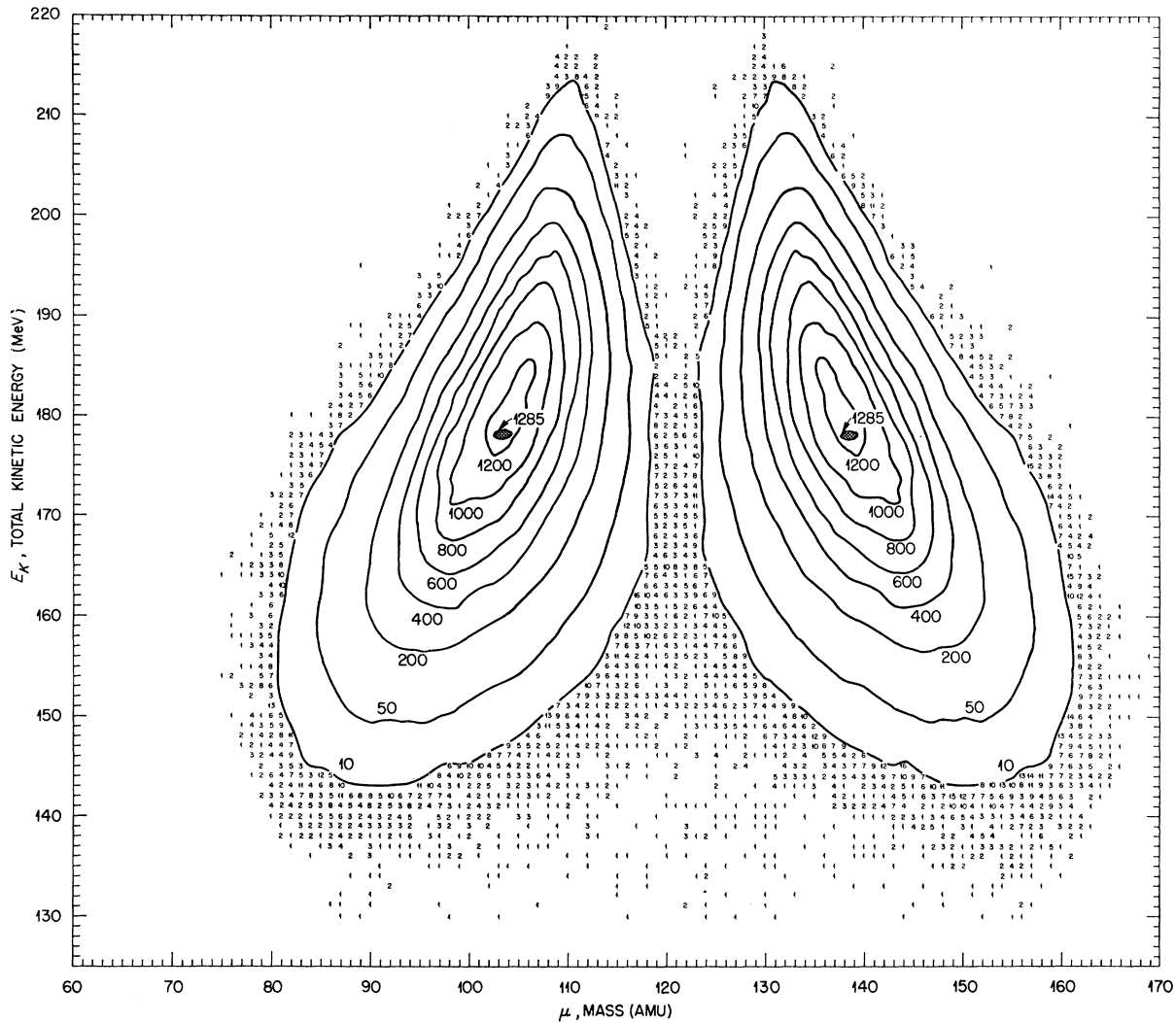$$Q = E_K^* + E_{x1}^* + E_{x2}^*, \qquad (2)$$

FIG. 6. Provisional mass-versus-total kinetic energy array $N(\mu,E_K)$ for ^{241}Pu thermal-neutron fission. Numbers labeling the contours and those entered outside the 10 contours indicate the number of events per cell (1 amu$\times$1 MeV).

where the E_{xi}^* represent the excitation energies of the primary (pre-neutron-emission) fragments. The ex-
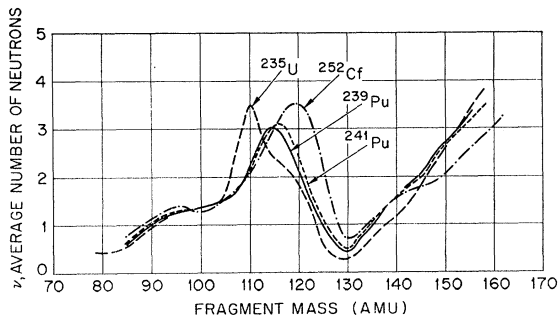

FIG. 7. Average number of neutrons $\nu(m^*)$ emitted as a function of fragment mass for several isotopes. Smooth curves are drawn for the thermal-neutron fission of ^{235}U and ^{239}Pu from the data of Ref. 3 and for ^{252}Cf spontaneous fission from the data of Ref. 19. The curve labeled ^{241}Pu is an estimate and is used in the ^{241}Pu derivations of $N(m^*)$ and $\langle E_K^*(m^*)\rangle$ from $N(\mu)$ and $\langle E_K(\mu)\rangle$.

citation energy E_{xi}^* appears, in turn, in the form of neutrons and gamma rays:

$$E_{xi}^*=\sum_{n=0}^{\nu} B_{ni}+\nu_i\eta_i+E_{\gamma i} \quad (i=1,2), \tag{3}$$

where B_{ni} is the binding energy of the nth neutron emitted from the ith fragment, η_i is the average center-of-mass kinetic energy of neutrons from the ith fragment, and $E_{\gamma i}$ is the energy of prompt gamma rays emitted from the ith fragment.

As in Ref. 1, we shall combine the average total kinetic energies obtained in the present experiment with the appropriate averages of the other quantities in Eqs. (2) and (3) to try to obtain a total-energy balance for the thermal-neutron fission of ^{239}Pu and ^{241}Pu.

For ^{239}Pu, the average number of neutrons as a function of primary fragment mass, $\nu(m^*)$, has been meas-
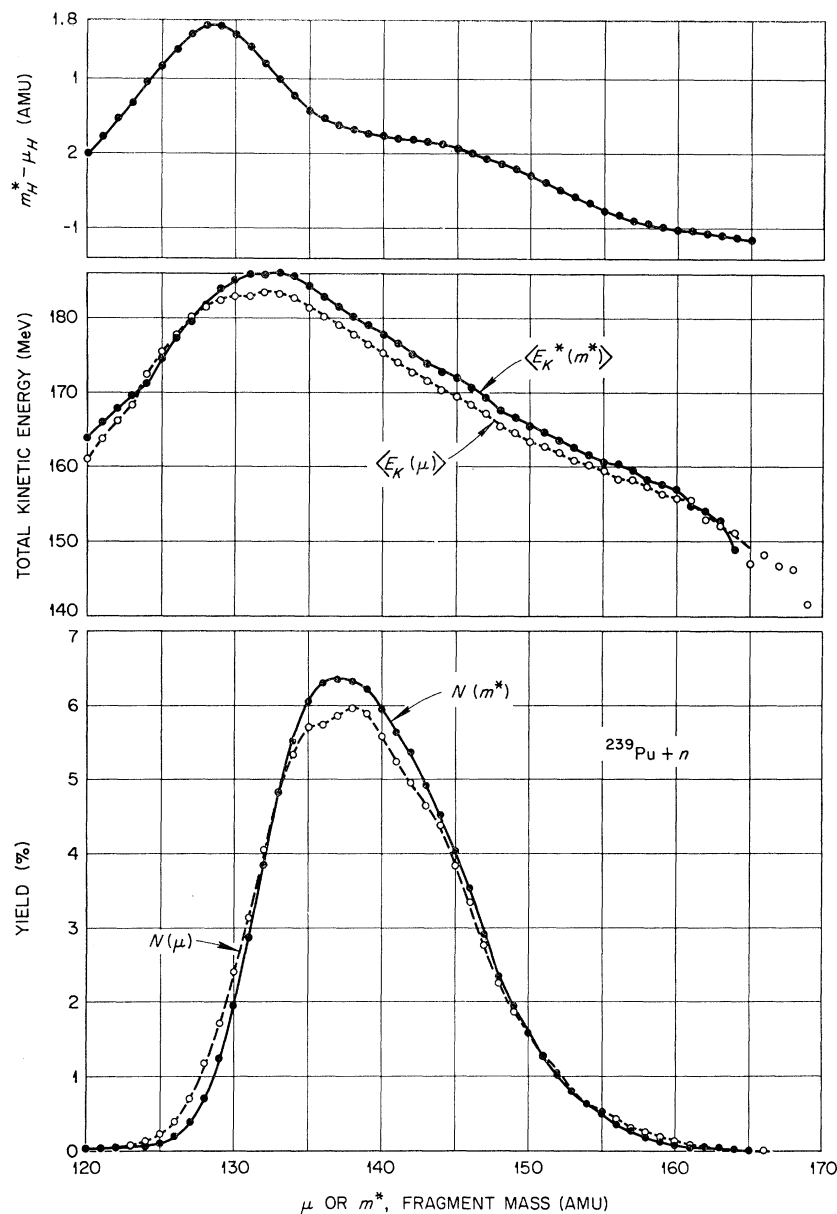
Fig. 8. Interim results for ^{241}Pu thermal-neutron fission. (a) Provisional-mass distribution $N(\mu)$ and pre-neutron-emission mass distribution $N(m^*)$. Statistical uncertainties are small; the peaks contain $>30\,000$ counts per amu. No corrections for resolution have been included. (b) $\langle E_K(\mu)\rangle$ and $\langle E_K^*(m^*)\rangle$. (c) $m_H^*-\mu_H$ versus m_H^*.

ured by Apalin et al.[3] The B_{ni} are obtained from semi-empirical mass formulas or tables; thus for a given fragment the total excitation energy appearing in the form of neutrons is given by the sum of the first two terms of Eq. (3). The total excitation energy E_{xT}^* for both fragments is given by $E_{x1}^*+E_{x2}^*$, or from Eq. (3),

$$E_{xT}^* = B_{N1}+B_{N2}+\nu_1\eta_1+\nu_2\eta_2+E_{\gamma T},   (4)$$

where B_{N1} and B_{N2} designate the sums of the neutron binding energies and where $E_{\gamma T}=E_{\gamma 1}+E_{\gamma 2}$. Thus the sum of the first two terms gives that part of the total excitation energy which appears in the form of neutron binding and is dependent on the particular mass formula

employed. The sum of the first four terms is the total part of E_{xT}^* which appears in the form of neutron emission, and $E_{\gamma T}$ is that part which appears in the form of gamma decay.

In Fig. 10 we have plotted the average total kinetic energy and various portions of the total excitation energy as functions of fragment mass for ^{239}Pu thermal-neutron fission. Calculations were carried out only for even-A fragments, and it was assumed that the associated atomic numbers were those which are energetically preferred. The curve labeled "neutron binding only" corresponds to the sum of the first two terms of Eq. (4) and is based on the neutron measurements of Apalin et al.[3] together with neutron binding energies
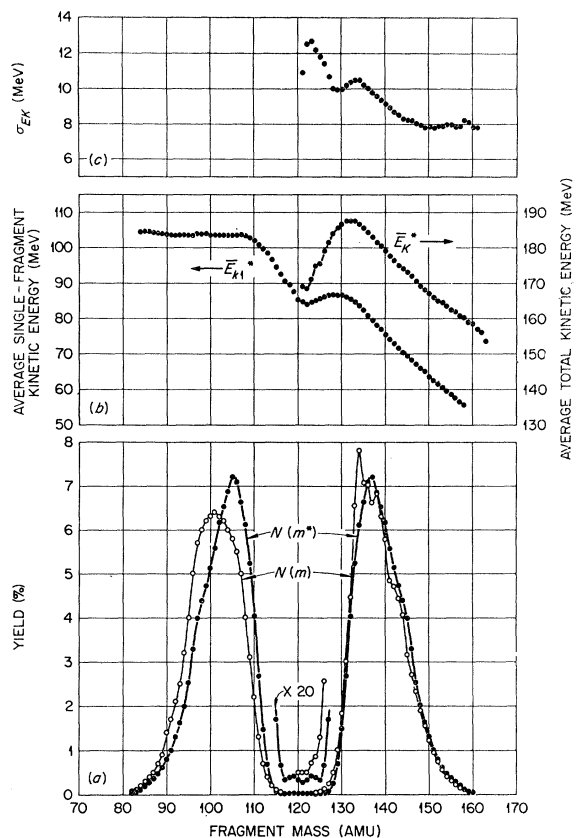
FIG. 9. Results for ²⁴¹Pu thermal-neutron fission. (a) Pre-neutron-emission mass distribution corrected for resolution; the post-neutron-emission mass yields shown are from Farrar *et al.* (Ref. 12). (b) Average single-fragment and total pre-neutron-emission kinetic energy as a function of fragment mass. (c) Root-mean-square width of total-kinetic-energy distribution as a function of fragment mass.

obtained from the Wing-Fong mass formula.[20] The curve labeled "neutrons" corresponds to the sum of the first four terms of Eq. (4), where we have assumed the average neutron kinetic energy η to be 1.3 MeV.[16] The curve labeled "gammas" corresponds to the last term of Eq. (4) and is estimated to be approximately one-half of the binding energy of the first neutron not emitted; for example, if $\nu = 2.0$ for fragment 1, the quantity $E_{\gamma 1}$ is estimated to be one-half of the binding energy of the third neutron. Since ν is in general not an integral value, suitable weighted averages are computed. The curve labeled "neutrons+gammas" is just the sum indicated and is an estimate of the total excitation energy $E_{xT}*$ for both fragments.

In the uppermost part of the figure we have plotted the "empirical Q," obtained from the sum of the experimental total-kinetic and excitation energies. For comparison, the Q values calculated from the Wing-Fong

²⁰ J. Wing and P. Fong, Phys. Rev. **136**, B923 (1964). Also J. Wing and J. Varley, Argonne National Laboratory Report No. ANL-6886, 1964 (unpublished).

mass formula for fission into even-A nuclei are plotted; the upper parabolas are obtained for even-Z, even-N fragments, the lower parabolas for odd-Z, odd-N fragments. The Q-values for fission into odd-A nuclei form a set of parabolas at energies between the two sets shown.

Similar calculations have been carried out for ²⁴¹Pu. The results are shown in Fig. 11. In this case there are no experimental values of $\nu(m*)$, hence the interpolated curve shown in Fig. 7 was used. The neutron kinetic energy η was assumed to be 1.3 MeV, as for ²³⁹Pu.

If the mass formula used in the calculation of Q values for fission into the various fragment species is accurate, and if the original nucleus divides predominantly into energetically preferred species, then the "empirical Q" curve would be expected to fall into an energy region approximately bounded by the highest Q values available for fission into even-even fragments at the upper edge and by the highest Q values available for fission into odd-odd fragments at the lower edge. In this respect, the agreement which is apparent in the upper portions of Figs. 10 and 11 is reasonably good. We observe the same features here, however, as in the case of ²⁵²Cf and ²³⁵U,[1] namely, that the rather strong decrease ($\sim$10 MeV) in empirical Q values at symmetry is not predicted by the mass formula. Similar
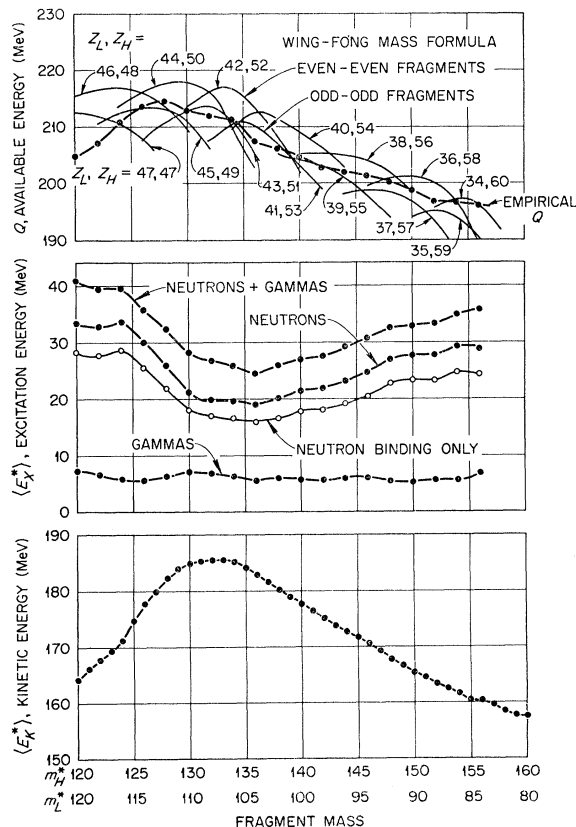

FIG. 10. Total-energy balance for ²³⁹Pu thermal-neutron fission. See text, Sec. V.

calculations based on the mass formulas of Myers and Swiatecki,[21] Seeger,[22] and Cameron[23] show similar trends, although the absolute Q values calculated from these formulas differ in some regions by several MeV; also, none seem to predict the rather strong decrease observed in empirical Q at symmetry.

It should not be inferred from the foregoing discussion that there is any *a priori* reason to prefer the Wing-Fong mass formula. We have chosen it for the representations of Figs. 10 and 11 partly because it gives best agreement with the Empirical Q values, and partly to be consistent with similar representations given previously for ^{235}U and ^{252}Cf.[1] We note again that the uncertainties in nuclear masses far off the stability line are large, and that differences in calculated Q values among various current mass formulas are as high as 5–10 MeV in some mass regions.

The appearance of fine structure in the average total kinetic energy versus fragment mass is weaker in the case of ^{239}Pu and ^{241}Pu than in the case of ^{235}U, as was also observed by Gibson *et al.*[7] Structure is perhaps a bit more apparent in the empirical Q function and is seen there to correspond generally to the structure of the calculated even-even "parabolas."[24] Excluding the near-symmetric mass region, a single exception seems to occur at 148–150 amu, where no dip appears in either empirical Q curve. The structure of the even-even parabolas shown in the figure is quite similar to that obtained when the Q values are calculated from the other mass formulas[21–23]; thus the qualitative correlation of locations of the fine-structure maxima with these parabolas is not dependent on the mass formula chosen for comparison.

Fine structure is also evident in the pre-neutron mass distributions for ^{239}Pu and ^{241}Pu [Figs. 4(a) and 9(a)], and again the locations of the fine-structure maxima are seen generally to coincide with the corresponding even-even parabolas in Q as calculated from a mass formula.

A comparison of the fine structure in the two fragment mass distributions (Fig. 12) indicates that the locations of the fine-structure maxima and minima occur at approximately the same heavy-fragment masses in the two cases, and not at the same light-fragment masses. This observation, while not particularly evident in the peaks, is especially evident in the valley and in the region at $m_H^* \cong 146$ amu. Thus it appears that the asymmetry term in the mass formula for the heavy
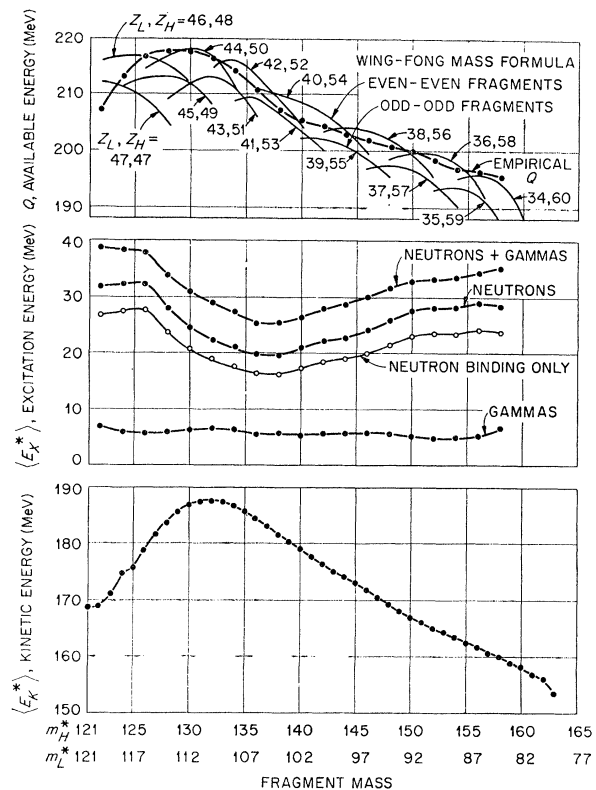
[21] W. D. Myers and W. J. Swiatecki, University of California Lawrence Radiation Laboratory Report No. UCRL-11980, 1965 (unpublished).

[22] P. A. Seeger, Nucl. Phys. 25, 1 (1961).

[23] A. G. W. Cameron and R. M. Elkin, Can. J. Phys. 43, 1288 (1965).

[24] The correlation of fine structure observed in fragment-mass distributions and average total kinetic energy with the even-even parabolas calculated from a mass formula was discussed by T. D. Thomas and R. Vandenbosch, Phys. Rev. 133, B976 (1964). Structure in the calculated Q was shown to originate in the asymmetry term of the mass formula, although the pairing term gives rise to the separation in energy of the Q parabolas for even-even, odd-odd, and odd-A fragment configurations.

FIG. 11. Total-energy balance for ^{241}Pu thermal-neutron fission. See text, Sec. V.

fragment indeed dominates in determination of the structure in Q.

With respect to the ^{239}Pu and ^{241}Pu mass distributions, we should like to point out the slight discrepancy which exists between the mass distributions reported here and those which we have reported previously.[8] The distributions of Ref. 8 were obtained before development of the mass-dependent pulse-height calibration for solid-state detectors[14] and were based on a single straight-line calibration normalized to time-of-flight energies. Although the change in over-all shape of either mass distribution is not large, it is significant enough to alter the detailed comparison of the distributions (see also Sec. VI). The more reliable mass-dependent calibration also has permitted the observation of fine structure as discussed above, not previously observed in the pre-neutron-emission fragment mass distributions. The details of the initial structure are altered slightly in the transformation from $N(\mu)$ to $N(m^*)$, and the structure observed at this point is enhanced somewhat by the correction for dispersion, as expected. These procedures, however, introduce no structure into the distributions which is not apparent initially.

The fine structure observed in $\sigma_{EK}(m^*)$ [Figs. 4(c) and 9(c)], although relatively weak, is correlated with that observed in the corresponding mass distribution, and again with the structure of corresponding calculated even-even parabolas in Q.

VI. THE FATE OF THE TWO EXTRA NEUTRONS

Since there is a difference of only two neutrons in the fissioning compound nuclei studied in this work, and since the compound-nucleus excitation energies are comparable in the two cases, it is of interest to ask: With respect to the fragments formed in ^{242}Pu* fission, from which fragment nuclei are the two neutrons removed in the fission of ^{240}Pu*? Or conversely: With respect to the fragments formed in ^{240}Pu* fission, to which fragments are the two neutrons added in the fission of ^{242}Pu*?

The answer is found immediately in Fig. 12: There we see the heavy-fragment mass distributions almost superimposed, while the light-fragment distributions are separated almost uniformly by two mass units. A cumulative-yield calculation of the type described by Terrell[16] shows little deviation from a difference of two neutrons in the light-fragment group.

A possible explanation for this observation lies in the special stability of the heavy-fragment group in low-excitation fission. It has often been pointed out in the literature that this group includes approximately the same range of masses, almost independent of the compound nucleus. This stability is clearly evident again in Fig. 12. A mechanism which results in this special stability with respect to the fate of the two extra neutrons in plutonium fission involves the neutron binding energies of the fragments, and in particular the two-neutron binding energies, as follows.

Let us imagine a configuration at the moment before scission consisting of basic fragment groups of nucleons, with the division of all protons and most of the neutrons complete, but with a few uncommitted neutrons remaining in the neck. It would then seem reasonable that the remaining neutrons fall, on the average, to the fragment whose neutron binding energy is higher.

Investigation of the neutron binding energies[21] shows that for $m_H \gtrsim 134$ amu the light-fragment binding energies are indeed larger than the appropriate heavy-fragment binding energies. This is not always the case for $m_H \lesssim 134$ amu; however, in this mass region the effects of closed shells become strong, and the mass
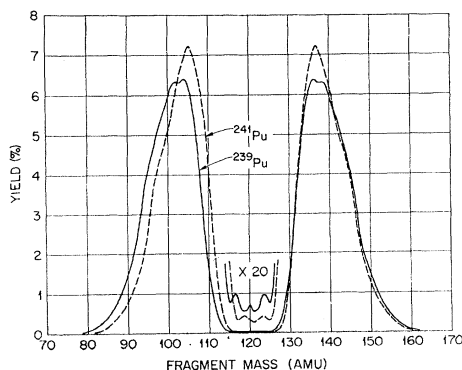

FIG. 12. Direct comparison of pre-neutron-emission mass Sistributions for ^{239}Pu and ^{241}Pu thermal-neutron fission. See decs. V and VI of text.

division appears to be governed almost entirely by these effects in the heavy fragment.

APPENDIX

In this Appendix we report energy calibration constants which may be generally useful in ^{239}Pu and ^{241}Pu thermal-neutron fission experiments with silicon solid state detectors.

The pulse-height–versus–energy relation given in Ref. 14 is

$$E = (a + a'm)x + b + b'm,$$

where E = fragment energy, m = fragment mass, and x = pulse-height or channel number. Let us re-emphasize here that the validity of this expression has been tested only over the range of masses and energies of fission fragments, and only for silicon detectors operated in the saturation region of the pulse-height–versus–detector-bias curve (see second paper listed in Ref. 14).

The calibration constants, a, a', b, b' may be expressed in terms of two points associated with the pulse-height spectrum. We choose these points to be P_L, the pulse height or channel number corresponding to the mid-point of a line drawn between the $\frac{3}{4}$-maximum points of the light-fragment group, and P_H, the pulse-height or channel number similarly corresponding to the mid-point of a line drawn between the $\frac{3}{4}$-maximum points of the heavy-fragment group.

Note that P_L and P_H need not be expressed as absolute pulse heights, but may be expressed as channel numbers or other units convenient to the experiment in question. It is required only that the pulse amplitude measuring system be linear over the range of amplitudes of the fission fragments.

Calibration constants for ^{252}Cf spontaneous fission (and also ^{235}U thermal-neutron fission) have been reported previously.[14] In the present work, comparison measurements of ^{239}Pu and ^{241}Pu thermal-neutron fission fragment spectra with ^{252}Cf spontaneous-fission fragment spectra, obtained with the same detector under identical operating conditions yielded the following values for the calibration constants:

	^{239}Pu$+n_{\text{thermal}}$	^{241}Pu$+n_{\text{thermal}}$
a	$27.6654/(P_L - P_H)$	$25.7402/(P_L - P_H)$
a'	$0.04106/(P_L - P_H)$	$0.03787/(P_L - P_H)$
b	$89.0064 - aP_L$	$88.5915 - aP_L$
b'	$0.1362 - a'P_L$	$0.1351 - a'P_L.$

Uncertainties in the fragment energies resulting from these constants are estimated to be ± 0.5 MeV.